Atomic Homodyne Detection of Weak Atomic Transitions

Mevan Gunawardena[1] and D. S. Elliott[1,2]

[1]School of Electrical and Computer Engineering, Purdue University, West Lafayette, Indiana 47907, USA
[2]Department of Physics, Purdue University, West Lafayette, Indiana 47907, USA

(Received 11 July 2006; published 22 January 2007)

We have developed a two-color, two-pathway coherent control technique to detect and measure weak optical transitions in atoms by coherently beating the transition amplitude for the weak transition with that of a much stronger transition. We demonstrate the technique in atomic cesium, exciting the $6s^2S_{1/2} \rightarrow 8s^2S_{1/2}$ transition via a strong two-photon transition and a weak controllable Stark-induced transition. We discuss the enhancement in the signal-to-noise ratio for this measurement technique over that of direct detection of the weak transition rate, and project future refinements that may further improve its sensitivity and application to the measurement of other weak atomic interactions.

DOI: 10.1103/PhysRevLett.98.043001 PACS numbers: 32.80.Qk, 32.60.+i, 32.80.Ys

The field of coherent control in atomic physics is based on the principles of interfering transition amplitudes. Numerous demonstrations of these have been reported in atomic [1,2], molecular [3], and condensed phase systems [4]. In this Letter, we describe our application of these coherent control interactions for the detection of weak optical transitions in atoms. This technique has a direct analog in homodyne or heterodyne detection, a coherent detection method commonly used to amplify weak electromagnetic signals [5] in the optical or radio frequency spectral regions. Use of an interference between transition amplitudes to detect a weak interaction in an atomic system has been reported previously, most notably in a series of measurements of magnetic dipole interactions [6–8], quadrupole interactions [9,10], and parity nonconserving (PNC) interactions [11–14]. In these works, a strong transition and the weak transition are each driven by the same optical field, and the interference between these amplitudes is used to effectively amplify the weak signal. The interference term is determined by reversing the symmetry of the experimental setup either by changing the directions of the dc fields or the polarization of the laser beam. In this Letter we discuss our demonstration of a technique of homodyne detection where two transition amplitudes are driven by two separate but mutually coherent laser fields. This distinction is significant in that it allows us to vary the interference condition by varying only the phase difference between the two optical fields. We demonstrate the technique in atomic cesium, concurrently exciting a strong two-photon transition and a weak controllable Stark-induced transition. With improvements in sensitivity and beam overlap, important for absolute measurements, the present technique could allow sensitive measurement of other weak optical interactions as well.

We show the excitation scheme used to demonstrate the homodyne detection technique in Fig. 1. We drive the $6s^2S_{1/2} \rightarrow 8s^2S_{1/2}$ transition in atomic cesium via two pathways, one of which is a strong two-photon interaction and the other a dipole-forbidden Stark-induced transition. The former is induced by the laser fundamental at frequency ω ($\lambda = 822.464$ nm), and the latter by the beam at twice this frequency, 2ω, i.e., $\lambda = 411.232$ nm. The amplitude and phase of these two fields are E^{ω} and ϕ^{ω}, and $E^{2\omega}$ and $\phi^{2\omega}$, respectively. By applying a static electric field of magnitude E_0 to the atoms in the interaction region, some P character is mixed into the S states, thus allowing the Stark-induced transition to take place. The net transition rate can be written as

$$W \propto |\mu^{(\omega)}(E^{\omega}e^{i\phi^{\omega}})^2 + \mu^{(2\omega)}E_0E^{2\omega}e^{i\phi^{2\omega}}|^2, \quad (1)$$

where $\mu^{(\omega)}$ and $\mu^{(2\omega)}$ are the transition moments for the two-photon and the Stark-induced transitions, respectively. Expanding this equation yields

$$W \propto |\mu^{(\omega)}(E^{\omega})^2|^2 + |\mu^{(2\omega)}E_0E^{2\omega}|^2 + 2Re[\mu^{(\omega)}\mu^{*(2\omega)}E_0(E^{2\omega})^*(E^{\omega})^2e^{i\Delta\phi}], \quad (2)$$

where $\Delta\phi = 2\phi^{\omega} - \phi^{2\omega}$ is the relevant phase difference between the two field components. The first term of this

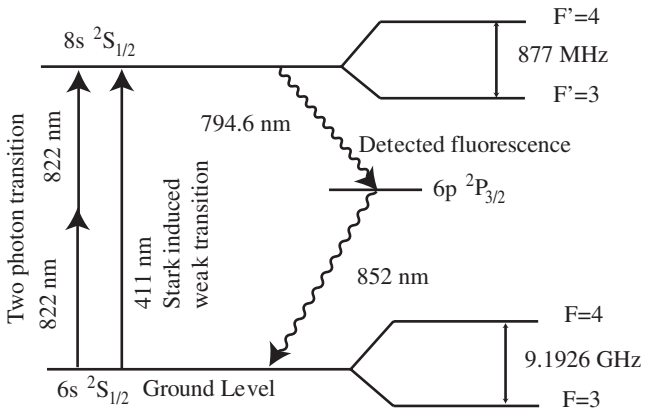

FIG. 1. Two pathways driving the $6s^2S_{1/2} \rightarrow 8s^2S_{1/2}$ transition in atomic cesium.

equation, corresponding to the two-photon transition rate, typically represents the largest component of the signal in our experiment, and serves as our "local oscillator" for the measurement. The second term in this expression is the rate of the Stark-induced transition by itself. The third term is the beat signal that arises due to the interference between the two-photon transition and the weak Stark-induced transition. We modulate the net excitation rate of the $8s^2S_{1/2}$ state by shifting the relative phase of the two frequency components of our optical beam, and use this modulation as a measure of the Stark-induced signal strength. Since the amplitude of this term is the geometric mean of the two other terms, it can be much greater than the term corresponding to the direct detection alone, and as we show later, can allow for shot-noise limited detection of extremely weak optical interactions.

The experimental setup is shown in Fig. 2. The primary laser source for the experiment is a stabilized cw Ti:sapphire laser, tuned to the two-photon resonance at 822 nm. We tune the laser frequency to either the $6s^2S_{1/2}F = 3 \rightarrow 8s^2S_{1/2}F' = 3$ or the $6s^2S_{1/2}F = 4 \rightarrow 8s^2S_{1/2}F' = 4$ transition frequency, differing from one another by 4.161 GHz. We have inserted a lithium triborate frequency-doubling crystal inside the laser cavity at one of the intracavity beam waists, generating the second-harmonic field at $\lambda = 411$ nm. The two beams pass through different arms of a Mach-Zehnder-like interferometer, as shown in Fig. 2. A half-wave plate placed in the UV path adjusts the polarization of the second harmonic, and a prism removes any residual 822 nm (ir) from the 411 nm (UV) beam. This latter element is necessary to eliminate the optical interference between the ir beams that might otherwise take place after the beams are recombined. By applying a linearly ramped voltage to the piezoelectric transducer (PZT) mirror mount in the ir branch of the interferometer, we can vary the relative phase $\Delta\phi$, controlling the net excitation rate as given by Eq. (2). We calibrate the displacement of the PZT versus the applied voltage by removing the wave plate and prism from the UV branch of the interferometer and observing the optical interference between the 822 nm beams traversing the two branches. We fit the displacement with a sixth-order polynomial, as it is somewhat nonlinear in the applied voltage.

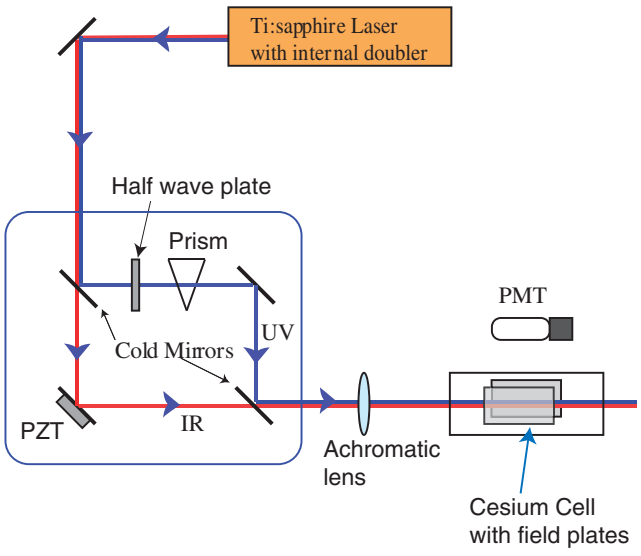

FIG. 2 (color online). Experimental setup. The Ti:sapphire laser includes an intracavity frequency-doubling crystal, producing phase coherent light at 822 nm and 411 nm. Varying the voltage applied to the piezoelectric transducer (PZT) allows us to vary the relative phase difference $\Delta\phi$.

We weakly focus the recombined beam into the cesium vapor cell using a 40 cm focal length achromatic doublet lens. The power levels of the 822 nm and 411 nm beams entering the cesium cell are ~150 mW and 20 μW, respectively. The confocal parameter of the focused beam is $z_0 \sim 10$ cm (ir and UV beam), and the $1/e^2$ beam diameters are ~350 μm (ir beam) and ~250 μm (UV beam). The cesium absorption spectrum is Doppler broadened to a full width at half maximum of 400 MHz (laser frequency units). The cell is fitted with a pair of internal rectangular stainless steel field plates of separation ~5 mm, to which we apply a bias of between 20 V and 5 kV. The direction of the dc field in the region between the plates is vertical, parallel to the polarization of the 822 nm and 411 nm beams. We collect and filter the 794.6 nm fluorescence emitted upon the decay of the excited state using lenses, mirrors, interference filters, and a spatial filter, and project this light onto the photocathode of a cooled photomultiplier tube (PMT). The collection efficiency of this setup, including the quantum efficiency of the PMT, is about 0.1%. The output pulses of this PMT (10 ns pulse duration) within successive 300 ms acquisition periods are counted, and the number of detected photons N stored in a laboratory PC. The photon count is proportional to the excitation rate of the $8s^2S_{1/2}$ state.

We collect each data set by measuring the fluorescence signal under varying conditions, and show an example in Fig. 3(a). The dc field strength is $E_0 = 4$ kV/cm and the laser is tuned to the $F = 4 \rightarrow F' = 4$ transition in this figure. The signal labeled (A) shows the level of the dark current counts, N_d, collected by blocking both the 822 nm and 411 nm beams. (B) represents the two-photon signal N_{TP}, as measured by tuning the 822 nm beam to the two-photon resonance and passing it through the cell, while blocking the UV beam. This signal also includes dark current N_d and a significant amount of 822 nm light scattered at the windows N_{sc}. For the signal labeled (C), we have blocked the ir beam, but allowed the UV beam to pass, driving the Stark-induced signal to yield $N_{\mathrm{SI}} + N_d$. The level of scattered light from the UV beam is undetectable in our experiment, so we do not include this term in (C). The signal level marked (D) represents the interference between the two-photon and Stark-induced signals. With both optical beams passing through the vapor cell, we

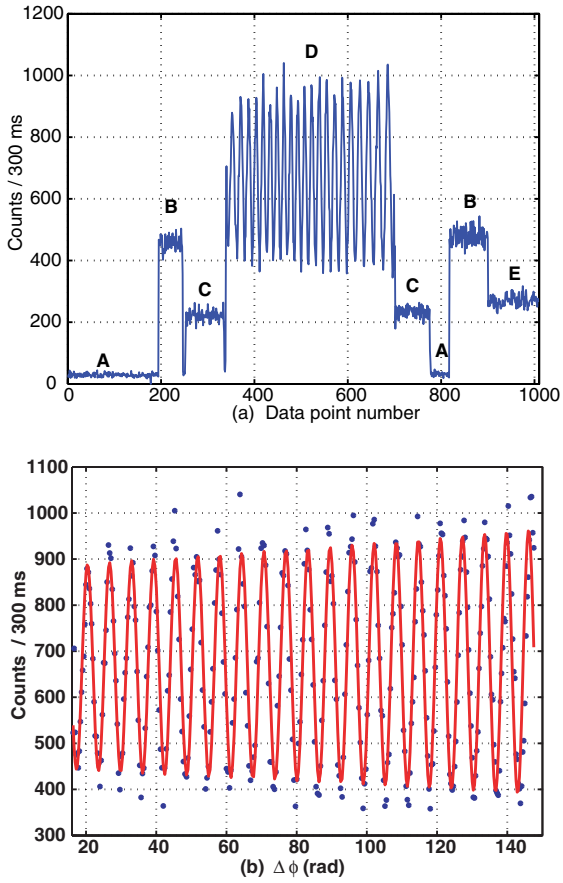

FIG. 3 (color online). A typical data set. E_0 for this run was 4 kV/cm. In (a), the labels on different segments of data indicate different input beams and/or frequencies, as described in the text. We show an enlargement of the beat signal, data segment (D), as well as the fitted sinusoid with varying amplitude, in (b).

vary the phase difference between the beams, modulating the total excitation rate according to Eq. (2). The average scan rate is quite slow for these measurements, $d\Delta\phi/dt \sim 1.2$ rad/ sec, to allow for an adequate signal count. Finally, the signal marked (E) in Fig. 3(a) represents the dark current and the noise level of the 822 nm light scattered by the windows, $N_d + N_{sc}$, measured by blocking the UV beam and tuning the ir beam away from the two-photon resonance.

We show an enlargement of the interference signal, i.e., section (D), in Fig. 3(b), as a function of $\Delta\phi$. The points represent the measured data, while the solid line is the result of a least squares fit of a sinusoid to the data. We allow the amplitude of the sinusoid to vary linearly with phase to account for small changes in the intensity, alignment, or overlap of the two laser beams. The rms deviation between the data and the sinusoid in this figure is 70 counts, somewhat larger than Poisson counting statistical fluctuations for an average signal of ~700 counts. We observe that the amplitude of the cross term in Eq. (2) does indeed vary linearly with the magnitude of the dc field E_0, and that

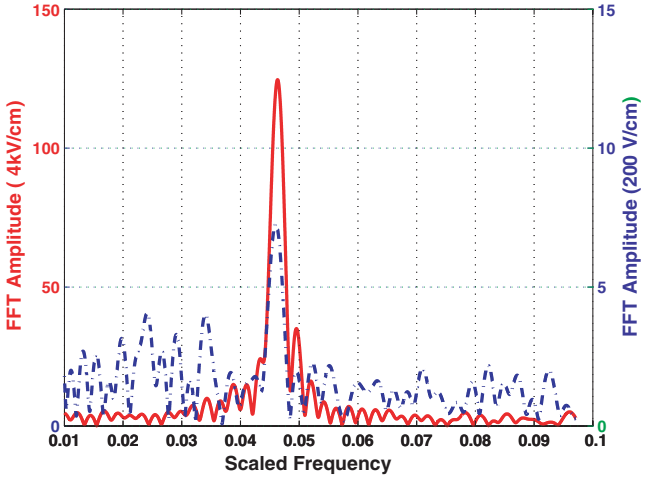

FIG. 4 (color online). Fourier transforms of the interference signals for the 4 kV/cm (solid line) and 200 V/cm (dot-dashed line) fields. The frequency is scaled, as explained in the text. The side lobes in the FFT of the 4 kV/cm data are artifacts of the finite number of data points.

the total signal is well described by the expression

$$N[\Delta\phi(V)] = N_{\mathrm{TP}} + N_{\mathrm{SI}} + N_d + N_{sc} + 2\eta\sqrt{N_{\mathrm{TP}}N_{\mathrm{SI}}}\cos[\Delta\phi(V)], \quad (3)$$

where V is the voltage applied to the PZT mirror mount in the interferometer, and η is a multiplier of order unity that accounts for imperfect matching of the wave fronts of the two laser field components. We were able to observe η as large as 0.9, but could not maintain this alignment with the mirror mounts available to us. Therefore, in practice, η was typically 0.6 to 0.75 for this weakly focused case. The beat signal is equally observable for the $F = 3 \rightarrow F' = 3$ and the $F = 4 \rightarrow F' = 4$ hyperfine components of the transition.

Another manner in which to view the data is through its Fourier transform. We show plots for two cases, with dc field strengths of 4 kV/cm (solid line) and 200 V/cm (dashed line) in Fig. 4. The frequency axis is scaled by the data acquisition time of 300 ms. While the signal-to-noise ratio for the latter case is certainly diminished in comparison with the former, it is still well above the detection limit. In contrast, the signal level for direct detection at 200 V/cm under the same conditions is well below the noise level.

For a total count of N fluorescence photons, the fluctuations in either signal alone, whether the Stark-induced or the two-photon interaction, are given by $\sqrt{N}$, consistent with Poisson statistics. For weak optical interactions, however, dark current and scattered light dominate the signal, and one must detect the fluorescence signal against this background. This is the regime where the homodyne detection offers the greatest potential. To see the improvement in the signal-to-noise ratio for homodyne detection versus direct detection, we examine

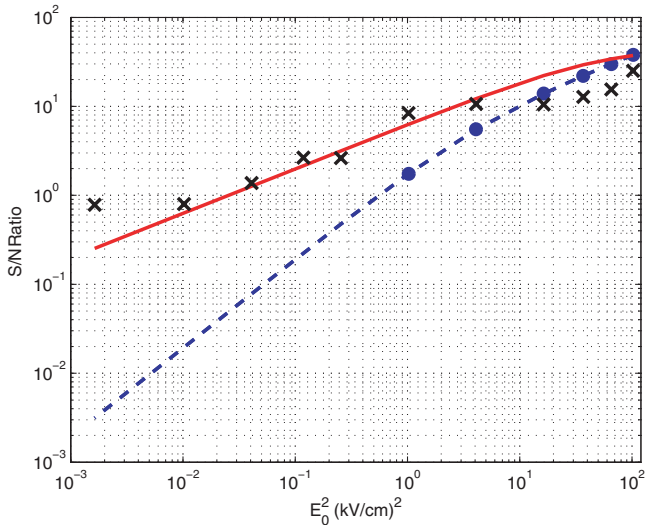

FIG. 5 (color online). Signal-to-noise ratio vs E_0^2 for Homodyne detection (×) and Direct detection (○), as determined from the data. The smooth lines are plots of Eqs. (4) and (5), using $N_{\mathrm{TP}} = 299$, $N_{\mathrm{SI}} = 14.7 \times E_0^2$, $N_d = 29$, and $N_{sc} = 205$.

$$S/N_{\mathrm{homodyne}} = \frac{2\sqrt{N_{\mathrm{TP}} N_{\mathrm{SI}}}}{\sqrt{N_{\mathrm{TP}} + N_{\mathrm{SI}} + N_d + N_{sc}}} \tag{4}$$

and

$$S/N_{\mathrm{direct}} = \frac{N_{\mathrm{SI}}}{\sqrt{N_{\mathrm{SI}} + 2N_d}}. \tag{5}$$

We show plots of measured S/N ratios, as well as Eqs. (4) and (5), in Fig. 5. For dc field strengths of 4 to 10 kV/cm, we observe comparable S/N ratios for the two detection schemes. With smaller fields, however, the signals decrease, linearly with E_0 for the homodyne signal, and quadratically for the direct detection signal. In the limit of strong local oscillator, i.e., N_{TP} greater than all other terms in Eq. (4), the S/N ratio for homodyne detection approaches $2\sqrt{N_{\mathrm{SI}}}$, as expected for shot noise limited detection, and S/N_{homodyne} then varies linearly with E_0. For direct detection, we can observe the absorption rate over the noise level only for $E_0 > \sim 1$ kV/cm. For comparison, the two smooth curves in Fig. 5 represent the S/N ratios given by Eqs. (4) and (5), using average counts $N_{\mathrm{TP}} = 299$, $N_{\mathrm{SI}} = 14.7 \times E_0^2$, $N_d = 29$, and $N_{sc} = 205$ from our data. The measured S/N ratios are in good agreement with these curves, showing that the sensitivity of our detection scheme is shot-noise limited. At the lowest dc field strength (40 V/cm) of our measurements, we project an increase in the signal-to-noise ratio for the homodyne detection over direct detection of 2 orders of magnitude.

There are several improvements one could envision to build upon the detection scheme we have described, including a higher efficiency fluorescence detector. Mirror mounts in the interferometer with a smoother adjustment and improved stability would allow us to achieve a factor of η closer to 1. Perhaps the most exciting possibility is to modulate the phase $\Delta\phi$ at a frequency in the kHz range, either by dithering the PZT mount, inserting an electro-optic modulator, or by introducing a slight frequency offset between the ω and 2ω beams, and use direct phase sensitive detection of the PMT signal using a lock-in amplifier. Data could then be collected in real time and with improved sensitivity. This scheme, along with several other improvements in sensitivity and gain, will be the goal of future works.

In summary, we have described a technique based upon a two-pathway coherent control interaction, using two distinct but coherently related laser fields, for detecting very weak optical interactions in atoms. This technique has features in common with optical heterodyne detection. We have demonstrated its capability for improved signal-to-noise ratios in detection of weak optical absorption signals, and reflect briefly upon potential avenues for improvements in this technique. This technique can be extended to measurement of other weak optical interactions, including quadrupole transitions, magnetic dipole transitions, and, if sensitivity and long-term stability allows, parity nonconserving transitions.

This material is based upon work supported by the National Science Foundation under Grant No. 0099477.

[1] C. Chen, Y.-Y. Yin, and D. S. Elliott, Phys. Rev. Lett. **64**, 507 (1990).
[2] Y.-Y. Yin, C. Chen, D. S. Elliott, and A. V. Smith, Phys. Rev. Lett. **69**, 2353 (1992).
[3] L. Zhu, V. Kleimean, X. Li, S. P. Lu, K. Trentelman, and R. J. Gordon, Science **270**, 77 (1995).
[4] E. Dupont, P. B. Corkum, H. C. Liu, M. Buchanan, and Z. R. Wasilewski, Phys. Rev. Lett. **74**, 3596 (1995).
[5] E. Voges, O. Ostwald, B. Schiek, and A. Neyer, IEEE J. Quantum Electron. **18**, 124 (1982).
[6] M. A. Bouchiat and L. Pottier, J. Phys. Lett. **37**, L-79 (1976).
[7] S. Chu, E. E. Commins, and R. Conti, Phys. Lett. **60A**, 96 (1977).
[8] S. L. Gilbert, R. N. Watts, and C. E. Wieman, Phys. Rev. A **29**, 137 (1984).
[9] L. R. Hunter, W. A. Walker, and D. S. Weiss, Phys. Rev. Lett. **56**, 823 (1986).
[10] P. K. Majumder and L. L. Tsai, Phys. Rev. A **60**, 267 (1999).
[11] P. S. Drell and E. D. Commins, Phys. Rev. A **32**, 2196 (1985).
[12] S. L. Gilbert, M. C. Noecker, R. N. Watts, and C. E. Wieman, Phys. Rev. Lett. **55**, 2680 (1985).
[13] M. A. Bouchiat, and L. Pottier, Science **234**, 1203 (1986).
[14] C. S. Wood, S. C. Bennett, D. Cho, B. P. Masterson, J. L. Roberts, C. E. Tanner, and C. E. Wieman, Science **275**, 1759 (1997).